Journal of Stress Analysis
Vol. 5, No. 1, Spring − Summer 2020, 1-10
Bu-Ali Sina University

ORIGINAL RESEARCH PAPER

A Numerical Method to Analyze the Brittle Fracture Using Phase-field Theory

M. Aghamohamadpour, S.H. Hoseini*
Faculty of Mechanical Engineering, Urmia University of Technology, Urmia, Iran.

Article info

Article history:
Received 10 January 2020
Received in revised form
10 March 2020
Accepted 06 May 2020

Keywords:
Brittle fracture
Crack propagation
Phase-field method
Finite element method

Abstract

Phase-field method is one of the recent developed fracture simulation methods which has attracted much interest in the last decade. Phase-field method can precisely simulate the crack nucleation as well as crack propagation path in complicated geometries. In general, phase filed method is a nonlocal theory that defines the cracks and other defects as a continuous part of the geometry with defining a length scale parameter. The major deficiency of this method is that it computationally is very time consuming. In this paper, a new numerical method based on finite element method was proposed to diminish the computational cost. The suggested numerical method was coded in Abaqus/Standard using an UEL subroutine. The simulations of different two-dimensional geometries demonstrate the capability of this method to predict the fracture process of brittle material. Results show that the proposed numerical method could significantly decrease the solution time in comparison to other methods.

Nomenclature

d	Phase field parameter	Γ	Fracture surface density
l_c	Length scale parameter	W	Elastic strain energy
W^+	Tensile contribution of the stored elastic strain energy	W^-	Compressive contribution of the stored elastic strain energy
$\boldsymbol{\varepsilon}$	Strain tensor	$\boldsymbol{\sigma}$	Stress tensor
G_c	Critical fracture energy per unit area	g	Degradation function
λ & μ	Lame constants	$\mathbf{u}$	Displacement vector
$\mathbf{b}$	Body force	$\mathbf{t}$	Traction vector
ρ	Density	$\mathcal{H}$	History parameter
$\boldsymbol{K}$	Element stiffness matrix	$\boldsymbol{R}$	Residual

1. Introduction

The fracture prediction of materials has attracted strong interest in the computational solid mechanics. Recently, phase-field method has demonstrated significant capability to simulate the fracture process. It has great ability to precisely determine the path of crack during propagation through minimizing an energy function. The phase-field method is a continuum approach that utilizes a diffuse representation of cracks in the place of actual discontinuities. Diffuse representation of cracks guarantees the continuous displace-

*Corresponding author: S.H. Hoseini (Assistant Professor)
E-mail address: s.hamedhoseini@yahoo.com
http://dx.doi.org/10.22084/JRSTAN-2001-1123
ISSN: 2588-2597

ment field and tackles some mathematical and computation obstacles. The geometry of diffuse crack is controlled by a length scale parameter which is an additional parameter of the fracture model.

Inability to describe the crack nucleation is the main limit of the fracture simulations which models discontinuities as a sharp crack. However, the phase field models have shown that they can be implemented in a straightforward numerical procedure, and have proved to precisely describe the fracture process from crack nucleation until final rapture. In phase field formulations, a continuous variable, designated the phase field parameter, is used to define a continuous shift between the broken and unbroken interfaces. This parameter is a scalar-valued damage quantity which with its gradients incorporated into the constitutive equation [1].

The phased field method was initially developed by Francfort and Marigo [2] to eliminate some restrictions associated with the Griffith theory of brittle fracture such as incapability to estimate crack initiation and branching, as well as predicting curved crack paths. They assumed that the total energy potential is a function of a surface term associated with the energy required for the creation of a crack. Then, this potential is minimized with respect to the displacement vector and the defused crack parameter. Further improvements were presented by Bourdin et al. [3, 4]; they proposed the regularization of the sharp crack geometry into a diffuse crack defined by introducing a scalar variable which gradually makes connection between cracked and intact states of the material. Kuhn and Müller [5] emphasized that the irreversible character of crack propagation should be incorporated into the phase field evaluation equation. They confirmed that the boundary value problem with the phase-field evolution equation produces an exponential solution type. Moreover, Kuhn and Müller [6] developed a new FE algorithm with exponential shape functions and showed that the suggested method make more precise results compared to the FE algorithm with Lagrange elements. Lancioni and Royer-Carfagni [7] suggested a modification of the function proposed by Bourdin et al. [3] to solve problems with deviatoric-type fracture. However, their model could not correctly simulate the inter-penetration and also crack-opening mode in the cases where the compressive stress is dominant. Amor et al. [8] improved the prior model by adding a degradation function to the spherical component of the stress. Significant improvements of this theory were carried out by Miehe et al. [9, 10]. They established a consistent thermodynamical background to model brittle fracture. Their model would be able to simulate the phase field evaluation as rate-independent or viscous material response. In particular, their formulation guarantees the irreversibility of crack propagation during the cyclic loading. Miehe et al. [9] in proposed a mixed finite element procedure where the coupled system of stress equilibrium and the phase-field evolution equations is solved simultaneously, while in the model by Miehe et al. [10] a numerical algorithm, namely a staggered scheme, was proposed to decouple the stress equilibrium and the phase-field evolution equations and a history parameter were introduced as a state variable to guarantee the irreversibility of crack growth.

Some researchers have demonstrated that the phase field approach can also be extended to simulate the dynamic fracture problems [11–15]. Furthermore, the phase field method has been implemented to simulate some attractive problems in the fracture mechanic fields. For example, Bourdin et al. [16] and Mikelic et al. [17] implemented the phase field method to model the hydraulic fracturing, Wilson et al. [18] simulated the failure of piezoelectric ceramics, Miehe and Schanzel [19] evaluated the rapture of rubbery polymers and Gültekin et al. [20] utilized the phase-field approach to estimate the arterial wall failure process. Some researchers also focused on solving the numerical difficulties and decreasing the computation time [21–25].

In this paper, a new numerical procedure is proposed to decrease the computational cost. The proposed numerical method was implemented in the commercial finite element Abaqus/Standard via an UEL subroutine. The fracture analysis of different 2D geometries exhibited the efficiency of this method to predict the fracture process of brittle material.

2. Governing Equation

2.1. Phase-field Formulation

In order to basically explain the phase field formulation, an infinitely extended $1D$ bar located along the x axis with a cross section Γ was considered. It was assumed that a diffusive crack exists in the middle of the bar at the axial position $x = 0$, Fig. 1a. The crack topology could be defined by a field variable $d \in [0, 1]$. In the phase field method, d which is designated as the phase-field parameter determines the amount of damage along the bar. The unbroken and the completely damaged state of the material are characterized with $d = 0$ and $d = 1$, respectively.

According to this idea, the non-smooth phase-field parameter can be approximated by an exponential function as [10]:

$$d\,(x) = e^{-\frac{|x|}{l_c}} \tag{1}$$

where l_c denotes the length scale parameter. The exponential function has the property that $d(0) = 1$ and $d(\pm\infty) = 0$. It is clear that Eq. (1) is the solution of the following differential equation which is subject to

the essential boundary conditions.

$$\begin{aligned} &d\left(x\right)-l_c^2 d^{''}\left(x\right)=0 \quad in \quad \Omega \\ &d\left(0\right)=1 \\ &d(\pm\infty)=0 \end{aligned} \tag{2}$$

Eq. (2) is the Euler equation of the following variational form [10]:

$$I\left(d\right)=\frac{1}{2}\int_{\Omega}(d^2+l_c^2 d^{'2})dV \tag{3}$$

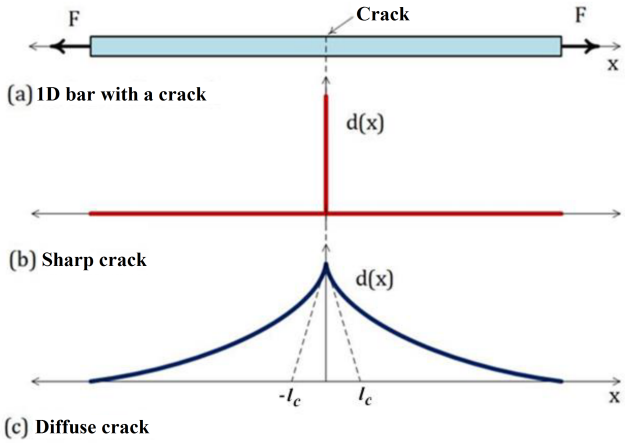

Fig. 1. Crack modeling in phase field method, a) 1D bar, b) Sharp crack at $x=0$ and c) Diffusive crack at $x=0$ modeled with the length scale l_c.

It can be easily calculated that the integration over 1D bar volume gives $I(d=e^{\frac{|x|}{l_c}})=l_c\Gamma$. Therefore, the fracture surface is related to the length scale parameter and fracture surface density could be introduced as [10]:

$$\begin{aligned} \Gamma\left(d\right)=\frac{1}{l_c}I\left(d\right)&=\frac{1}{2l_c}\int_{\Omega}(d^2+l_c^2 d^{'2})dV \\ &=\int_{\Omega}\gamma(d,d^{'})dV \end{aligned} \tag{4}$$

where $\gamma\left(d,d^{'}\right)$ is the crack surface density defined as a function of the phase-field parameter and its spatial gradient. The multidimensional form of crack surface density can be expanded as below [10]:

$$\gamma\left(d,\nabla d\right)=\frac{1}{2l_c}d^2+\frac{l_c}{2}\left|\nabla d\right|^2 \tag{5}$$

Crack surface density has a significant role in the estimation of fracture process. Based on phase field theory, the sharp crack surface geometry inside a solid, as illustrated in Fig. 1b, could be modeled with a diffusive crack, visualized in Fig. 1c. Fig. 2 schematically illustrates a discrete and a diffusive crack in a 3D body. As can be seen in Fig. 2, the internal discontinuity is regularized by a diffusive topology governed by defining a scalar valued parameter.

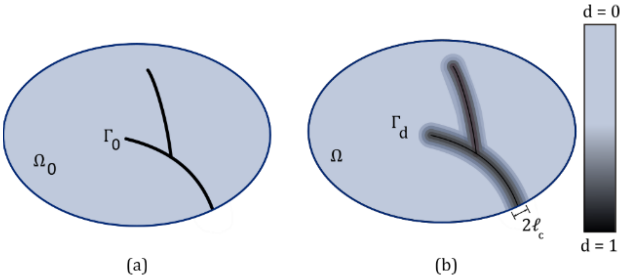

Fig. 2. Phase-field modeling, a) Discrete crack surface b) Diffusive crack surface.

Taking the advantage of the above-outlined definition of the regularized crack, a time-dependent fracture evolution law could be established. This evolution is achieved using an energetic description as outlined below. Describing the damaged material based on Griffith's theory of brittle fracture, the stored energy can be express as [26]:

$$\Psi(\varepsilon,\Gamma)=\int_{\Omega}W(\varepsilon(\mathbf{u}))\,\mathrm{d}\Omega+\int_{\Gamma}G_c\,\mathrm{d}\Gamma \tag{6}$$

where W and $\boldsymbol{\varepsilon}$ are the elastic strain energy and the strain tensor, respectively. Γ is the boundary of crack and G_c is the critical fracture energy per unit area. To evaluate the crack initiation and propagation, the stored energy, Eq. (6), should be minimized. Ambati et al. [1] suggested the following phase-field approximation of Eq. (6):

$$\Psi(\boldsymbol{\varepsilon},d)=\int_{\Omega}g(d)W(\varepsilon)\,\mathrm{d}\Omega+\int_{\Gamma}G_c\,\mathrm{d}\Gamma \tag{7}$$

where $g(d)$ is a degradation function which controls the elastic strength reduction. To overcome the numerical complications, Bourdin et al. [4] proposed the following approximation for the second term of Eq. (7):

$$\int_{\Omega}G_c\gamma(d,\nabla d)\,\mathrm{d}\Omega\approx\int_{\Gamma}G_c d\Gamma \tag{8}$$

where γ, crack surface density, is defined based on Eq. (5). It is obvious that cracks heal during compressive loading. Therefore, it is proposed to decompose the elastic strain energy to tensile and compressive terms [8–10]. The suggested approximation takes the following form

$$\begin{aligned} \Psi\left(\boldsymbol{\varepsilon},d\right)=&\int_{\Omega}\left\{g\left(d\right)W^{+}+W^{-}\right\}\,\mathrm{d}\Omega \\ &+\int_{\Omega}G_c\gamma\left(d,\nabla d\right)\,\mathrm{d}\Omega \end{aligned} \tag{9}$$

where W^{+} and W^{-} denote the tensile and compressive contribution of the stored elastic strain energy, respectively. In order to define the tensile contribution, Miehe et al. [10] introduced the positive and negative part of the strain tensor as:

$$\boldsymbol{\varepsilon}=\boldsymbol{\varepsilon}_{+}+\boldsymbol{\varepsilon}_{-} \tag{10}$$

This is the spectral decomposition of the strain tensor based on its principal values and directions. These parts are defined as [10]:

$$\boldsymbol{\varepsilon}_+ = \sum_{i=1}^{n} \langle \varepsilon_i \rangle_+ \mathbf{n_i} \otimes \mathbf{n_i} \tag{11}$$

$$\boldsymbol{\varepsilon}_- = \sum_{i=1}^{n} \langle \varepsilon_i \rangle_- \mathbf{n_i} \otimes \mathbf{n_i} \tag{12}$$

where ε_i and $\mathbf{n_i}$ are i-th principal strain and the principal strain direction, respectively. The bracket operators are defined as $\langle x \rangle_+ := (x + |x|)/2$ and $\langle x \rangle_- := (x - |x|)/2$. Based on Eqs. (11) to (12), tensile and compressive part of the stored elastic strain energy could be determined as [10]:

$$W^+ = \frac{\lambda}{2} \langle tr\varepsilon \rangle_+^2 + \mu \varepsilon_+ : \varepsilon_+ \tag{13}$$

$$W^- = \frac{\lambda}{2} \langle tr\varepsilon \rangle_-^2 + \mu \varepsilon_- : \varepsilon_- \tag{14}$$

where λ and μ are Lame constants for elastic response. It should be emphasized that both terms are positive and the volumetric contribution is either positive or negative according to the sign of the trace of strain tensor.

The degradation function, $g(d)$, has a significant role in the phase-field formulation. It determines the material responses to changes in the phase field parameter. It is assumed to have the properties that $g(0) = 1$, $g(1) = 0$ and $g^{'}(1) = 0$. In this work, Quadratic degradation function was implemented which is defined as [10]:

$$g(d) = (1 - d)^2 + \kappa \tag{15}$$

where κ is a scalar parameter chosen to be so small that avoids the numerical problem when the phase field parameter reaches unity. Quadratic degradation function is a simple function which has been most widely implemented in the literature [4].

2.2. Minimizing the Phase-field Formulatio

In this section, the governing equations of the phase field method is derived based on the global energy rate balance principle. At the beginning, the rate of external work is defined as [27]:

$$P_{ext} = \int_{\partial\Omega} \mathbf{t}, \dot{\mathbf{u}} d\partial\Omega + \int_{\Omega} \mathbf{b}, \dot{\mathbf{u}} d\Omega \tag{16}$$

where $\mathbf{u}$ is the displacement vector. $\mathbf{b}$ and $\mathbf{t}$ are the body force and traction vector applied to the boundary, respectively. For dynamic response, the kinetic energy functional is given by [27]:

$$\mathcal{K} = \int_{\Omega} \frac{1}{2} \rho \dot{\mathbf{u}} \cdot \dot{\mathbf{u}} d\Omega \tag{17}$$

where ρ is the density. According the first law of thermodynamics and neglecting the dissipation, the balance of energy can be written as [27]:

$$\dot{\mathcal{K}} + \dot{\Psi} - P_{ext} = 0 \tag{18}$$

Substituting Eq. (9) and Eqs. (16) to (17) into Eq. (18) and using Eq. (5), the rate of internal work funsction for the phase field theory could be obtained. After applying the divergence theorem, the balance of energy can be presented as [27]:

$$\begin{aligned} &\int_{\Omega} [-\boldsymbol{\nabla}, \boldsymbol{\sigma} - \mathbf{b} + \rho \ddot{\mathbf{u}}] \cdot \dot{\mathbf{u}} d\Omega \\ &\quad + \int_{\Omega} [g^{'}(d) W^+ + \frac{G_c}{l_c} d + G_c l_c \Delta d] \dot{d} d\Omega \\ &\quad + \int_{\partial\Omega} [\boldsymbol{\sigma}, \mathbf{n} - \mathbf{t}] \cdot \dot{\mathbf{u}} d\partial\Omega \\ &\quad + \int_{\partial\Omega} [2 G_c l_c \nabla d . \mathbf{n}] \cdot \dot{d} d\partial\Omega = 0 \end{aligned} \tag{19}$$

where $\partial\Omega$ and Δ are the boundary surrounding the material and Laplace operator, respectively. It is assumed that the Eq. (19) must hold for arbitrary values of $\dot{\mathbf{u}}$ and $\dot{d}$. Therefore, the strong form for the phase field initial boundary value problem is obtained as [27]:

$$\boldsymbol{\nabla} . \boldsymbol{\sigma} - \mathbf{b} + \rho \ddot{\mathbf{u}} = 0 \tag{20}$$

$$\frac{G_c}{l_c} d - G_c l_c \Delta d = -g^{'}(d) W^+ \tag{21}$$

where

$$\boldsymbol{\sigma} = g(d) \frac{\partial W^+}{\partial \boldsymbol{\varepsilon}} + \frac{\partial W^-}{\partial \boldsymbol{\varepsilon}} \tag{22}$$

Also, the following boundary conditions are gained:

$$\begin{aligned} &\boldsymbol{\sigma}\mathbf{n} = \mathbf{t} && \text{on} && \partial\Omega_t \\ &\nabla d \cdot \mathbf{n} = \mathbf{0} && \text{on} && \partial\Omega \\ &\mathbf{u} = \overline{\mathbf{u}} && \text{on} && \partial\Omega_u \end{aligned} \tag{23}$$

Displacement vector and traction are prescribed on $\partial\Omega_u$ and $\partial\Omega_t$, respectively; $\mathbf{n}$ is the outward unit normal vector of the boundary. The initial conditions are given by $\mathbf{u}_0$ for displacements, $\dot{\mathbf{u}}_0$ for velocities.

It should be mentioned that the above formulation does not prevent cracks healing when loads are removed. To enforce the irreversibility of crack propagation during unloading, Miehe et al. [10] proposed to replace the strain energy in the phase-field equation, Eq. (21), by a history parameter, $\mathcal{H}$, which has a role like a threshold parameter and satisfies the Kuhn–Tucker loading/unloading conditions [10]:

$$W^+ - \mathcal{H} \leq 0, \quad \dot{\mathcal{H}} \geq 0, \qquad \dot{\mathcal{H}}(W^+ - \mathcal{H}) = 0 \tag{24}$$

In the monotonically increasing load, using the history parameters or tensile contribution of the stored elastic strain energy has no effect on the results. On the other hand, disregarding the history parameter does not make any thermodynamic inconsistencies.

3. Numerical Simulation

In this section, a new numerical technique is suggested for the phase field method based on the Eq. (20) and Eq. (21). The numerical procedure is coded in the finite element method software ABAQUS by a user defined element subroutine (UEL). In UEL subroutine, in each increment the displacement vector and incremental displacement vector of each node are available. This makes it possible to define the tensile and compressive parts of the stored elastic energy in each iteration of an increment, Eqs. (13) to (**??**). With defining W^+, Eq. (21) becomes a linear differential equation of phase field parameter and could be easily solved. So, the phase field differential equation, Eq. (21), would be decoupled from Eq. (20) and each equation could be solved separately. This split scheme is named staggered method in literature [10].

The Galerkin finite element method is utilized to develop a numerical procedure. The weak form of Eq. (21) could be established by multiplying an appropriate weighting function, η, to Eq. (21) and applying the divergence theorem as:

$$\int_\Omega \left[\left(1+\frac{2W^+l_c}{G_c}\right)\mathrm{d}\eta + l_c^2\nabla d,\nabla\eta\right]\mathrm{d}\Omega = \int_\Omega \left(\frac{2W^+l_c}{G_c}\right)\eta\,\mathrm{d}\Omega \quad (25)$$

In the Galerkin finite element procedure, it is most common practice to use same approximation for the weight functions and the trial solutions. Therefore, in the UEL subroutine for each element the phase field parameter d and weight function are discretized as (for convenience, a matrix notation is used):

$$\begin{aligned} d &= [N]\{d\} \\ \eta &= [N]\{\eta\} \end{aligned} \quad (26)$$

where $[N]$ denotes the shape function which is a row matrix of n components associated with the number of nodes in an element; $\{d\}$ and $\{\eta\}$ are $n\times 1$ vectors of the phase-field parameter and weighting function values at each node, respectively. The corresponding gradient of Eq. (26) can be given by:

$$\begin{aligned} \nabla d &= [B]\{d\} \\ \nabla\eta &= [B]\{\eta\} \end{aligned} \quad (27)$$

where B is a matrix with spatial derivatives of the corresponding shape function row matrix. Substituting Eqs. (26) and (27) into Eq. (25), the following equation is gained.

$$[K]^{dd}\{d\} = \{F\} \quad (28)$$

where

$$\begin{aligned} [K]^{dd} &= \int_\Omega \left[\left(1+\frac{2W^+l_c}{G_c}\right)[N]^T[N] + l_c^2[B]^T[B]\right]d\Omega \\ \{F\} &= \int_\Omega \left(\frac{2W^+l_c}{G_c}\right)[N]^T d\Omega \end{aligned} \quad (29)$$

Solving Eq. (28) using 4-nodes quadrilateral isoparametric elements, the phase-field parameter value at each node could be estimated. All integrals in Eq. (28) were calculated using the nine-point Gaussian quadrature rule. The numerical results show that the reduced integration scheme does not converge for Eq. (28). By calculating the phase-field parameter value at each node, the average value of the phase-field parameter, d_{av}, is defined for each element and incorporated into the Eq. (27). Therefore, the weak form of the stress equilibrium is defined by implementing the appropriate weighting function and applying the divergence theory to Eq. (20). Discretizing the displacement vector similar to phase field parameter, $\mathbf{u} = [N]_u\{u\}, \nabla\mathbf{u} = [B]_u\{u\}$, the following residual can easily be calculated:

$$\begin{aligned} \boldsymbol{R} &= \boldsymbol{F}_{int} - \boldsymbol{F}_{ext} \\ &= \int_\Omega [B]_u^T\boldsymbol{\sigma}d\Omega - \int_\Omega [N]_u^T\boldsymbol{b}d\Omega - \int_\Omega [N]_u^T\boldsymbol{t}d\Omega \end{aligned} \quad (30)$$

Based on Miehe et al. [9], stress tensor is introduced as:

$$\begin{aligned} \boldsymbol{\sigma} = &\left[(1-d_{av})^2+\kappa\right] \\ &\sum_{i=1}^{3}\left[\lambda\langle\varepsilon_1+\varepsilon_2+\varepsilon_3\rangle_+ + 2\mu\langle\varepsilon_i\rangle_+\right]\mathbf{n_i}\otimes\mathbf{n_i} \\ &+\sum_{i=1}^{3}\left[\lambda\langle\varepsilon_1+\varepsilon_2+\varepsilon_3\rangle_- + 2\mu\langle\varepsilon_i\rangle_-\right]\mathbf{n_i}\otimes\mathbf{n_i} \end{aligned} \quad (31)$$

Furthermore, the stiffness matrix for each element could be determined as:

$$\boldsymbol{K} = \int_\Omega \left[(1-d_{av})^2+\kappa\right][B]_u^T[D][B]_u d\Omega \quad (32)$$

where [D] is the element stiffness matrix. Using reduced integration scheme, the residual vector and stiffness matrix can be calculated. Abaqus employs an incremental-iterative strategy utilizing the Newton–Raphson approach to determine the displacement of all nodes of model. On the other hand, for each increment the solution procedure iterates until the phase field parameter and the displacement field converge. Fig. 3 shows the flowchart of the proposed numerical method.

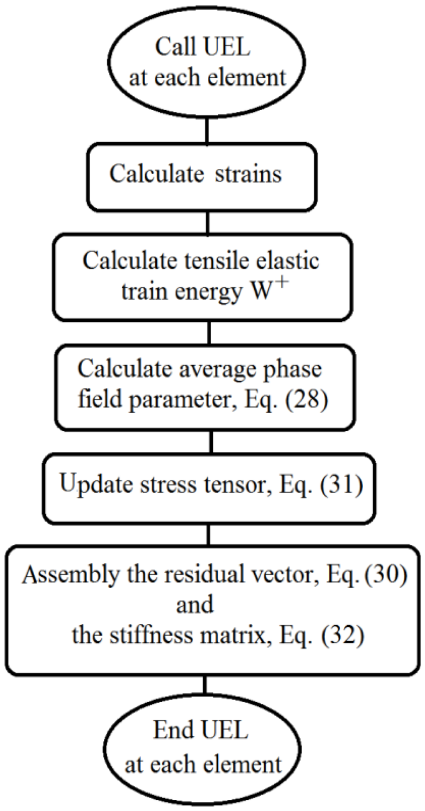

Fig. 3. Flowchart of the proposed numerical method.

4. Results

First of all, the simplest case, which is a 2D plane strain element, was considered to examine the effect of phase field parameter on material response. The dimensions of this element was 1×1mm in x and y direction. The bottom nodes were constrained in y direction and nodes on a vertical side were constrained in x direction. The opposite vertical side gradually underwent 0.02mm displacement in the x direction, then the applied displacement was removed. Subsequently, 0.1mm displacement was applied in the x direction. The Young's modulus was set to $E = 210\text{kN/mm}^2$ and the Poisson's ratio to $\nu = 0.3$. The critical energy release rate was $G_c = 5\text{N/mm}$ and the length scale parameter was $l_c = 0.1\text{mm}$.

Fig. 4 displays the effect of the phase field parameter on the material response. As can be seen in Fig. 4a, the strength of material decreases while the phase field parameter increases. It is also obvious that the model has good agreement with the results introduced by Miehe et al. [10] for a similar element. The phase field parameter curves will be exactly equal and the discrepancy between stress-strain curves is less than 1 percent. Furthermore, the model satisfies the irreversibility of crack propagation during unloading and also the phase filed parameter remain constant during unloading process.

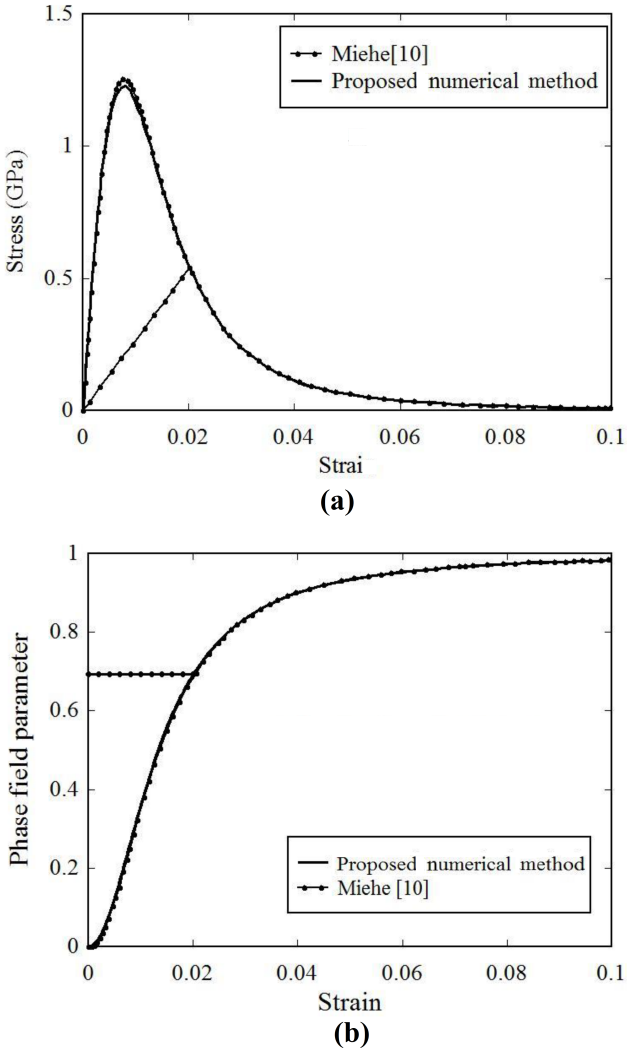

Fig. 4. a) Stress- strain curve and b) Phase field parameter- strain curve for a unit square element

The proposed numerical model converges with maximum increment size in comparison with other method proposed in the literature. Fig. 5 displays the effect of increment number on the response of a square element mentioned above. As can be seen in Fig. 5a, the results converge for increment number more than 20. But, in the numerical method proposed by Molnár and Gravouil [21], the convergence is not achieved for increment number less than 1000. It shows the capability of the proposed model to introduce results with small number of increments and consequently decreases the computational time. Table 1 compares the estimated error of the maximum value of the stress-stress curves with different increment number. The error is defined as the maximum discrepancy from the results introduced by Miehe et al. [10]. These results show that the proposed model could capture the material behavior with the minimum number of increments. This means that this method could decrease the computational cost.

To examine the proposed numerical method to pre-

dict the fracture process of the brittle fracture, the well-known single edge notched tensile sample was considered. The geometry of the sample was a unit square containing an edge notch, Fig. 6a. The length of the notch was a half of the square size with the distance between the opposite faces of the notch tip equal to h. With decreasing the size of h, the notch geometry coincides with the theoretical crack geometry. The boundary conditions are defined as the bottom side of the specimen is fixed, while the top side is moved. The FEM model of the specimens is depicted in Fig. 6b.

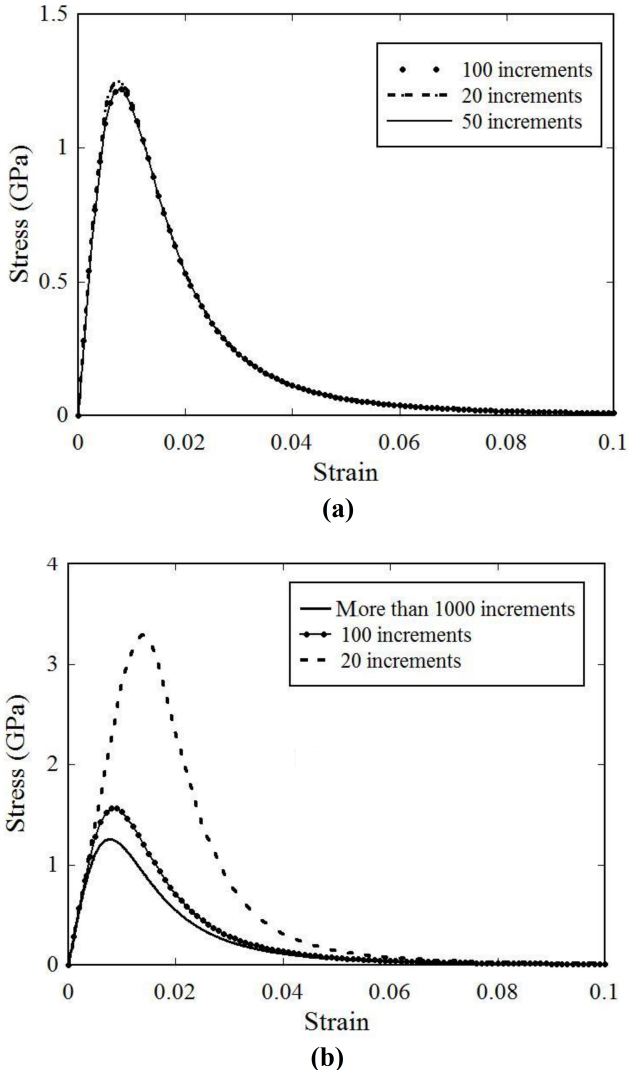

Fig. 5. Stress-strain curve for unit square under one dimensional extension a) The proposed numerical method, b) The staggered method proposed by Molnár and Gravouil [21].

Table 1
The error of the stress-stress curves with different increment number.

Number of increments	Proposed model	Molnár and Gravouil [21]
20	3%	166%
100	1%	21%
1000	1%	2%

The region around the notch path is refined in order to reach the mesh size equal to h. As can be seen in this figure, when the applied load reaches the maximum value, the crack initiates propagation horizontally. Fig. 6e displays that the results converge when the minimum size of mesh, h, decreases; and insignificant discrepancy is observed between mesh size equal to 0.002 and 0.002mm.

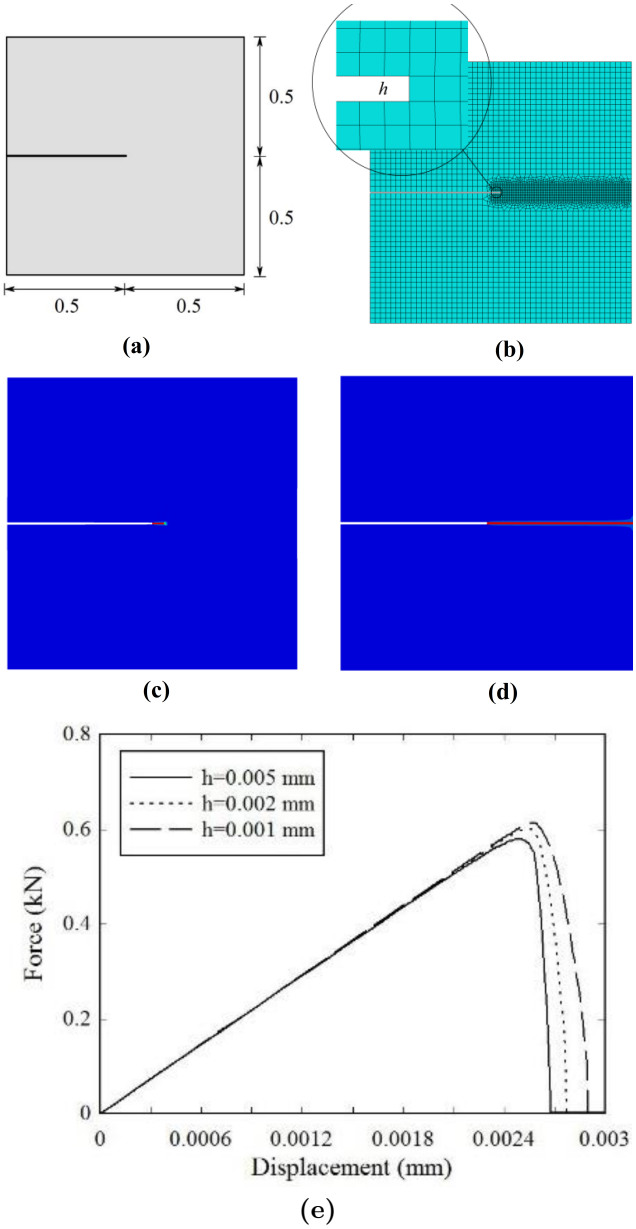

Fig. 6. Fracture analysis of single edge notched tensile sample.

Fig. 7a shows the dependency of the results on increment number. As can be seen in Fig. 7, the differences are negligible when the number of increments is more than 1000 and the maximum load carrying capacity is approximately the same. In Fig. 7b the reaction force is shown for the tensile specimens for different length scale parameters (l_c). It can be seen

that the maximum value of reaction force reduces when the length scale parameter increases. Furthermore, by increasing the length scale parameter the results gradually converge.

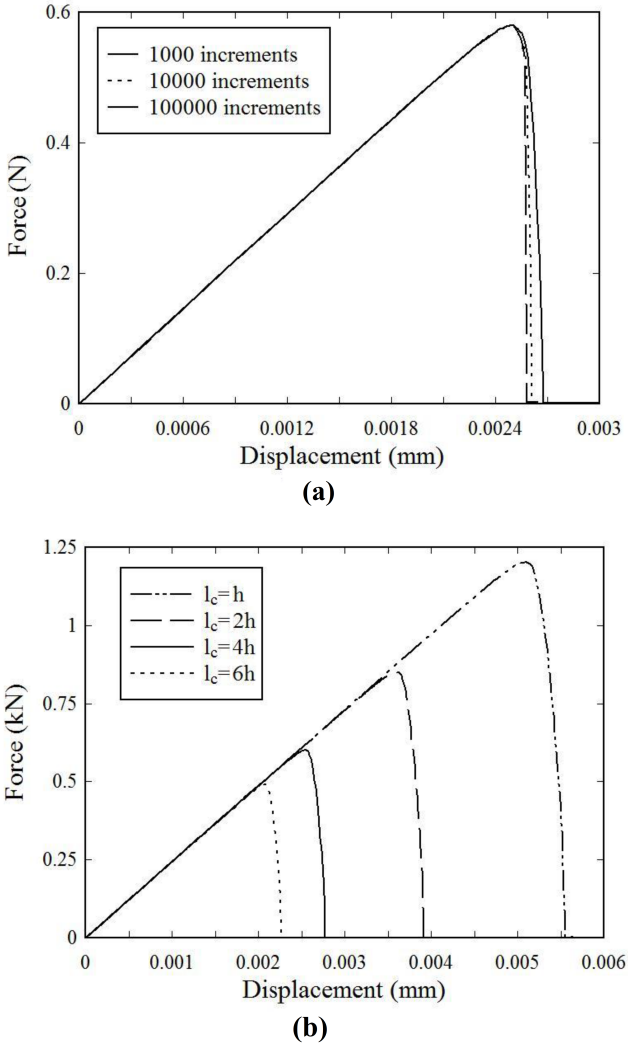

Fig. 7. Dependency of the results on a) Increments size, and b) Length scale parameter.

To examine the utility of the new numerical implementation to predict the fracture process of complex geometries, an asymmetric double notch specimen was used. The exact geometry is illustrated in Fig. 8a. The material properties are $E = 210\text{kN/mm}^2$, $\nu = 0.3$, $lc = 0.1\text{m}$, $g_c = 5\text{N/mm}$. The mesh is well refined and has the size of $h = 0.002\text{mm}$ around the notch. The tensile deformation is implemented by applying displacement on the top boundary of the sample. The bottom side of the sample is fixed. The simulated fracture process and crack path is shown in Fig. 8b. The obtained crack propagation path pattern is in excellent agreement with the results proposed by Molnár and Gravouil [21]. Furthermore, the proposed method can simulate the slender pattern of crack propagation which is more realistic than the Molnar pattern.

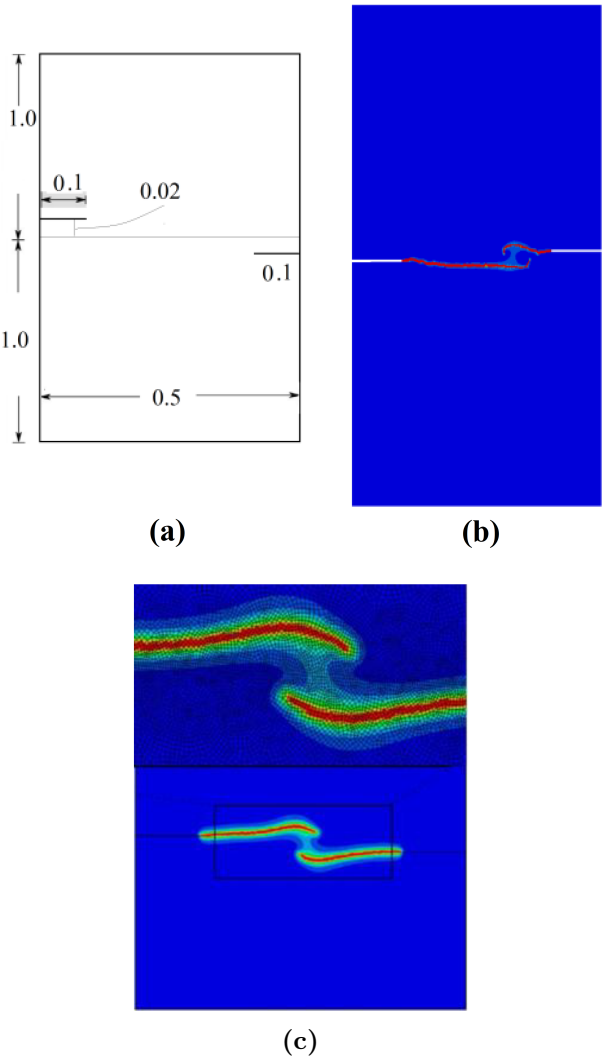

Fig. 8. a) Geometry of the double notched asymmetric tensile test, b) Crack propagation pattern based on proposed method, and c) Molnar method [21].

Fig. 9 demonstrates the fracture process in the plate with double circular notches. These samples do not have any pre-existing cracks. The material properties are $E = 210\text{kN/mm}^2$, $\nu = 0.3$, $lc = 0.1\text{m}$, $g_c = 5\text{N/mm}$. The mesh is well refined and has the size of $h = 0.002\text{mm}$ around the notch. The tensile deformation is implemented by applying displacement on the top boundary of the sample. The bottom side of the sample is fixed. The simulated fracture process and crack path is shown in Fig. 9. Fig. 9a shows the path of crack propagation in the plate with double symmetric circular notches and Fig. 9b shows path in the plate with double asymmetric circular notches. The results proves that the suggested numerical technique can precisely predict the fracture processed without modelling any pre-existing crack in the samples.

The final model considered in this paper is a notched plate, with load application by a top pin and a fixed lower pin, and with a hole offset from the center to induce mixed-mode fracture. This test was experimen-

tally implemented by Ambati et al. [1]. The geometry of the sample is depicted in Fig. 10a. The material was cement mortar, composed of 22% cement 66% sand and 12% water. The material is expected to behave linearly elastic until brittle fracture occurs. The Yong Modulus, Poisson's ratio, and critical energy release rate are $E = 6\text{kN/mm}^2$, $\nu = 0.22$, and $g_c = 2.28\text{N/mm}$, respectively. The fractured specimen is displayed in Fig. 10b. A curved crack develops from the notch to the large hole. Later, a secondary straight crack appears from the hole to the sample edge. The numerical simulations were performed with with a length scale parameter $lc = 0.1\text{mm}$. The mesh consists of quadrilateral elements with refinement in the areas where the crack is likely to propagate. As can be seen in Figs. 10c and 10d, simulations could precisely capture the experimentally observed crack pattern.

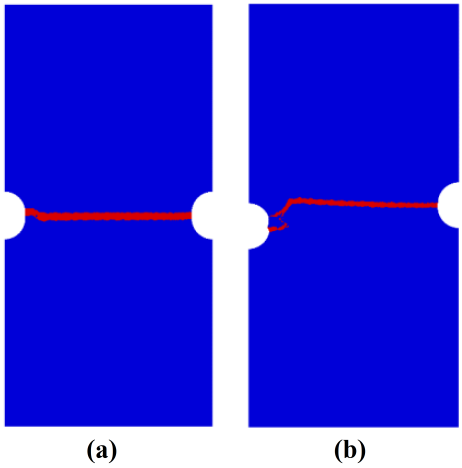

Fig. 9. Crack propagation pattern based on proposed method for a) Plate with double symmetric circular notches, and b) Plate with double asymmetric circular notches.

5. Conclusions

In this paper a numerical procedure based on FEM was proposed to simulate the phase-field theory. The numerical algorithm was implemented in the commercial FE code Abaqus/Standard to simulate brittle fracture in 2D solids. The numerical procedure was coded in the context of a user defined element subroutine.

The method is based on the minimizing the rate-independent variational form of the stored energy in the material. The equilibrium and the phase field equation were decoupled and solved separately. The connection was established using a so-called history variable, which contains the materials elastic potential energy.

The utility of the method is shown through several examples. It was shown that the result could converge based on the proposed method for large increment size. This decreases the computational cost of the phase field theory. Moreover, there is no need to severely decrease the element size . Sufficient amount of meshes could capture the material response.

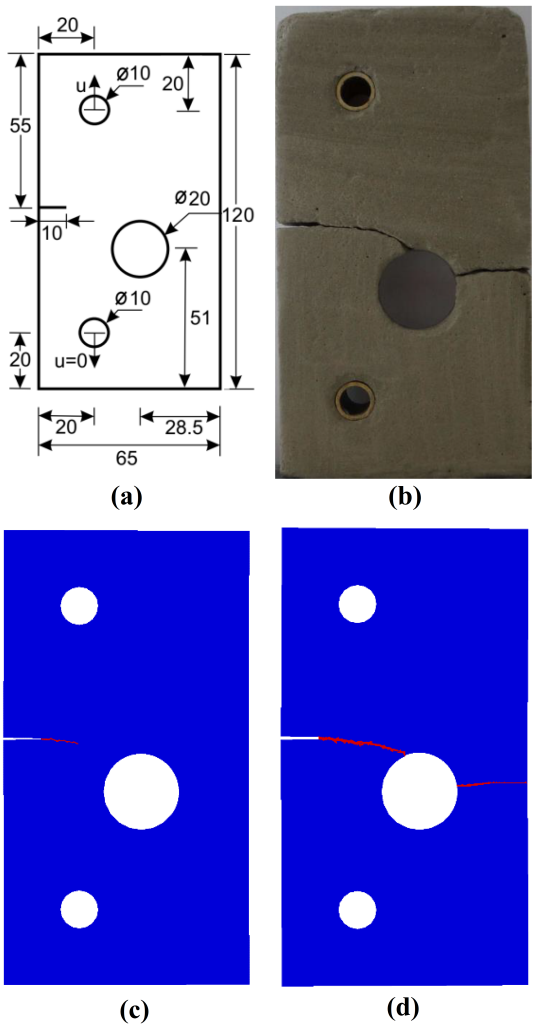

Fig. 10. a) Geometry of the notched plate, b) The fractured specimen, c) Crack initiation, and d) Final fracture based on the proposed method.

References

[1] M. Ambati, T. Gerasimov, L. De Lorenzis, A review on phase-field models of brittle fracture and a new fast hybrid formulation, Comput. Mech., 55 (2014) 383-405.

[2] G. Francfort, J.J. Marigo, Revisiting brittle fracture as an energy minimization problem, J. Mech. phys. Solids, 46(8) (1998) 1319-1342.

[3] B. Bourdin, G.A. Francfort, J.J. Marigo, Numerical experiments in revisited brittle fracture, J. Mech. phys. Solids, 48(4) (2000) 797-826.

[4] B. Bourdin, G.A. Francfort, J.J. Marigo, The variational approach to fracture, J. Elast., 91 (2008) 5-148.

[5] C. Kuhn, R. Müller, A continuum phase field model for fracture, Eng. Fract. Mech., 77(18) (2010) 3625-3634.

[6] C. Kuhn, R. Müller, A new finite element technique for a phase field model of brittle fracture, J. Theor. Appl. Mech., 49(4) (2011) 1115-1133.

[7] G. Lancioni, G. Royer-Carfagni, The variational approach to fracture mechanics. A practical application to the French *Panthon* in Paris, J. Elast., 95(1-2) (2009) 1-30.

[8] H. Amor, J.J. Marigo, C. Maurini, Regularized formulation of the variational brittle fracture with unilateral contact: Numerical experiments, J. Mech. phys. Solids, 57(8) (2009) 1209-1229.

[9] C. Miehe, M. Hofacker, F. Welschinger, A phase field model for rate-independent crack propagation: Robust algorithmic implementation based on operator splits, Comput. Methods Appl. Mech. Eng., 199(45-48) (2010) 2765-2778.

[10] C. Miehe, F. Welschinger, M. Hofacker, Thermodynamically consistent phase-field models of fracture: Variational principles and multi-field FE implementations, Int. J. Numer. Methods Eng., 83(10) (2010) 1273-1311.

[11] C.J. Larsen, Models for dynamic fracture based on griffith's criterion, In: Hackl. (eds) IUTAM symposioum on variational concepts with applications to the Mechanics of Materials, IUTAM Bookseries, Vol. 21, Springer, Dordrecht, (2010).

[12] C.J. Larsen, C. Ortner, E. Suli, Existence of solutions to a regularized model of dynamic fracture, Math. Methods Models Appl. Sci., 20(7) (2010) 1021-1048.

[13] B. Bourdin, C.J. Larsen, C.L. Richardson, A time-discrete model for dynamic fracture based on crack regularization, Int. J. Fract., 168(2) (2011) 133-143.

[14] M.J. Borden, C.V. Verhoosel, M.A. Scott, T.J.R. Hughes, C.M. Landis, A phase-field description of dynamic brittle fracture, Comput. Methods. Appl. Mech. Eng., 217-220 (2012) 77-95.

[15] M. Hofacker, C. Miehe, A phase field model of dynamic fracture: Robust field updates for the analysis of complex crack patterns, Int. J. Numer. Methods Eng., 93(3) (2013) 276-301.

[16] B. Bourdin, C.P. Chukwudozie, K. Yoshioka, A variational approach to the numerical simulation of hydraulic fracturing, In Proceedings of the 2012 SPE Annual Technical Conference and Exhibition, volume SPE 159154, Society of Petroleum Engineers Publisher, (2012).

[17] A. Mikelic, M.F. Wheeler, T. Wick, A phase-field method for propagating fluid-filled fractures coupled to a surrounding porous medium, Multiscale Model. Simul., 13(1) (2015) 367-398.

[18] Z.A. Wilson, M.J. Borden, C.M. Landis, A phase-field model for fracture in piezoelectric ceramics, Int. J. Fract., 183(2) (2013) 135-153.

[19] C. Miehe, L.M. Schanzel, Phase field modeling of fracture in rubbery polymers. part I: Finite elasticity coupled with brittle failure, J. Mech. Phys. Solids, 65 (2014) 93 -113.

[20] O. Gültekin, H. Dal, G.A. Holzapfel, A phase-field approach to model fracture of arterial walls: theory and finite element analysis, Comput. Methods Appl. Mech. Eng., 312 (2016) 542-566.

[21] G. Molnár, A. Gravouil, 2D and 3D Abaqus implementation of a robust staggered phase-field solution for modelling brittle fracture, Finite Elem. Anal. Des., 130 (2017) 27-38.

[22] P. Zhang, X. Hu, X. Wang, W. Yao, An iteration scheme for phase field model for cohesive fracture and its implementation in Abaqus, Eng. Fract. Mech., 204 (2018) 268-287.

[23] T.K. Mandal, V.P. Nguyen, Jian-Ying Wu, Length scale and mesh bias sensitivity of phase-field models for bbrittle and cohesive fracture, Eng. Fract. Mech., 217 (2019) 106532.

[24] K. Seleš, T. Lesičar, Z. Tonković, J. Sorić, A residual control staggered solution scheme for the phase-field modeling of brittle fracture, Eng. Fract. Mech., 205 (2019) 370-386.

[25] J. Fang, C. Wu, T. Rabczuk, C. Wu, C. Ma, G. Sun, Q. Li, Phase Field Fracture in Elasto-plastic Solids: Abaqus implementation and case studies, Theor. Appl. Fract. Mech., 103 (2019) 102252.

[26] M.J. Borden, T.J.R. Hughes, C.M. Landis, A. Anvari, I.J. Lee, A phase-field formulation for fracture in ductile materials: Finite deformation balance law derivation, plastic degradation, and stress triaxiality effects, Comput. Methods Appl. Mech. Eng., 312 (2016) 130-166.

[27] M.J. Borden, T.J.R. Hughes, C.M. Landis, C.V. Verhoosel, A higher-order phase-field model for brittle fracture: Formulation and analysis within the isogeometric analysis framework, Comput. Methods Appl. Mech. Eng., 273 (2014) 100-118.